Kinetics of copper nanoparticle precipitation in phosphate glass: An isothermal plasmonic approach

Journal:	*Physical Chemistry Chemical Physics*
Manuscript ID:	CP-ART-10-2014-004662.R1
Article Type:	Paper
Date Submitted by the Author:	06-Nov-2014
Complete List of Authors:	Sendova, Mariana; New College of Florida, Division of Natural Sciences Jimenez, Jose; University of North Florida, Chemistry; New College of Florida, Physics Smith, Robert; New College of Florida, Physics Rudawski, Nicholas; University of Florida, Materials Science and Engineering

Kinetics of copper nanoparticle precipitation in phosphate glass: An isothermal plasmonic approach

Mariana Sendova, *[†] *José A. Jiménez*[*,‡] , *Robert Smith,* [†], *Nicholas Rudawski*[✗]

[†]Optical Spectroscopy & Nano-Materials Lab, New College of Florida, Sarasota, FL 34243, USA

[‡]Department of Chemistry, University of North Florida, Jacksonville, FL 32224, USA

[✗]Major Analytical Instrumentation Center, University of Florida, Gainesville, FL 32611, USA

Abstract

The kinetics of copper nanoparticle (NP) precipitation in melt-quenched barium-phosphate glass has been studied by *in situ* isothermal optical micro-spectroscopy. A spectroscopically based approximation technique is proposed to obtain information about the activation energies of nucleation and growth in a narrow temperature range (530 – 570 °C). Pre-plasmonic and plasmonic NP precipitation stages are identified separated in time. The process as a whole is discussed employing classical nucleation/growth theory and the Kolmogorov−Johnson−Mehl−Avrami phase change model. Activation energies of 3.9(7) eV and 2.6(5) eV have been estimated for the pre-plasmonic and plasmonic spectroscopically assessed stages, respectively. High resolution transmission electron microscopy, differential scanning calorimetry, and Raman spectroscopy were used as complementary techniques for studying the nanoparticulate phase and glass host structure. An empirical linear dependence of the diffusion activation energy on the glass transition temperature with broad applicability is suggested.

*E-mail: sendova@ncf.edu (M.S.), jose.jimenez@unf.edu (J.A.J.)

Introduction

Materials consisting of noble metal nanoparticles (NP) embedded in a dielectric host have garnered much interest due to their nonlinear optical properties and potential applications across a wide range of topics including photonics[1], sensing[2], solar cells[3], and antibacterial composites[4,5]. The plasmonic nanocomposites are traditionally prepared by introducing metal ions along with a reducing agent into an optically transparent host matrix. Upon heat treatment (HT), the reduction of the metal from the ionic to atomic species promotes the precipitation of NPs within the host.[6-8] The optical properties of these materials depend on the NPs' size distribution, morphology, and interaction with one another, which are determined not only by the metal concentration, but by the material's processing as well.[6,8-10] In order to effectively tailor these properties, a general understanding of NP formation and development are required such that the appropriate processing parameters can be chosen to yield NPs which create the desired optical properties.

While the optical properties caused by Cu NPs have been reported for a variety of host media,[11-14] real-time kinetics of Cu NP nucleation and growth in a robust solid-state inorganic matrix have not been reported yet. *In situ* optical microspectroscopy has been recently proposed by the authors for the real-time study of metal transport and NP growth kinetics, based on the plasmonic response of the nanocomposites to thermal processing[10,15,16]. Yet, to this point, studies have been only devoted to Ag NPs in films and glasses, opening the possibility to extend to other metals and matrices.

There are likely two main reasons yielding experimental challenges that the study of Cu NPs presents. Admittedly, the development of Cu NPs is commonly suppressed or inhibited because of the more significant susceptibility of copper to oxidation, relative to other noble metals (silver, gold). A glass-synthesis solution to this problem which is employed in the present work is the incorporation of a reducing agent (tin) together in the matrix. The second challenge is related to the extinction spectral features. Due to the relatively low energy threshold of the interband transitions in Cu, the surface plasmon resonance (SPR) of Cu NPs is asymmetric, substantially dampened, and with enhanced extinction in the high energy photon range. Such Cu NP spectroscopic features make difficult the application of the traditional Ag NP analysis based on SPR peak position and full-width at half maximum (FWHM) correlating with NP size. This

study proposes an alternative quantitative method overcoming the inherent spectroscopic challenges.

Hence, in this work, Cu-doped phosphate glasses are studied for the first time by real-time *in situ* optical micro-spectroscopy. Analyses of the SPR of small (diameter < 10 nm) developing Cu NPs were used to assess the processes of NP nucleation and growth. Within the context of homogeneous steady-state nucleation theory[17] and the Kolmogorov−Johnson−Mehl−Avrami (KJMA) theory[18-20] of phase transformations, the free energy barrier for nucleation and the activation energy for copper precipitation within the host matrix were estimated. Differential scanning calorimetry and Raman spectroscopy are ultimately employed as characterization tools in an attempt to correlate the kinetic data with material structural and thermal properties.

Experimental

Phosphate glasses consisting of a $50P_2O_5$:50BaO (mol%) composition and doped with 10 mol % of each the NP precursor compound CuO and the reducing agent SnO were prepared by the melt-quenching technique (10Cu/Sn).[21] Prior to the kinetic measurements the samples were annealed at 450 °C in air for one hour using a Linkam THMS600 heating stage. The heating rate was 10 °C/min. The annealing temperature used is the glass transition temperature, T_g of the glass. The chosen annealing temperature was intended to be high enough to relieve some of the internal stress of the samples caused by the melt-quenching preparation, while low enough to avoid unwanted NP precipitation or nucleation. The reported T_g values in this study are measured by a TA Instruments Q20 differential scanning calorimeter (DSC) at a heating rate of 20 °C/min.

The final, polished samples studied were approximately 0.5 mm thick. A CRAIC Technologies QDI 2010 micro-spectrophotometer (MSP) equipped with a Xe short-arc lamp and the heating stage described above was used to conduct isothermal *in situ* optical absorption measurements in air at five different temperatures (10-degree interval from 530 °C to 570 °C). In order to rapidly attain isothermal conditions, the samples were heated at a rate of 100 °C/min. Measurements were performed with a 10× objective on 102 μm × 102 μm sample areas. Particular attention was given to maintain sample position during experiments. Absorption

spectra were taken every two minutes after reaching the target HT temperature, for up to 5 hrs, until samples became opaque.

Raman spectra were acquired using a Leica DMLP microscope coupled to a Raman system from Kaiser Optical Systems Inc. The RamanRxn1™ analyzer incorporates the thermoelectrically-cooled charge-coupled device detector for maximum sensitivity, Invictus™ near infrared semiconductor laser with wavelength of 532 nm and holographic grating to provide fast, simultaneous full spectral collection of Raman data. The spectral resolution of the Raman system is about 5 cm^{-1}.

A JOEL2010F transmission electron microscope operating at 200 kV was used to directly image and quantify the shape and size of the NPs using conventional high-resolution transmission electron microscopy (HRTEM) imaging. Specimens for HRTEM analysis were prepared using an FEI DB235 dual scanning electron microscope/Ga^+ focused ion beam (FIB) system using methods described elsewhere[22]. The final stages of specimen preparation during FIB milling were performed using a 5 keV Ga^+ beam to minimize the damage layer imparted to the specimen[23]. HRTEM imaging was performed over an area of ~25 μm^2 for each FIB-prepared specimen. ImageJ © analysis software was used to quantify the size distribution of NPs for each specimen using the collected HRTEM images.

Results and discussion

The extinction spectra were analyzed within the photon energy range of 1.75-2.50 eV, as shown in Fig. 1. The Cu NPs' SPR peak absorption is ~ 2.15 eV.[24] The exact position is sensitive to the NPs' size, shape and dielectric function of the matrix.[25,26] Fig. 1 illustrates the extinction spectra development in 4-min intervals 560 ^oC. Only half of the acquired spectra for the sample were presented in Fig. 1 for clarity. A gradual rise of the SPR is noticed with time. An analogous time evolution is measured at all isothermal settings. From spectroscopic standpoint, each isothermal family of spectra can be divided in two consecutive-in-time spectral subsets. Such division is inherent of the optical spectroscopy method employed herein. More importantly, it is proposed that by considering a two-stage copper precipitation process, the quantitative precipitation discussion (*vide infra*) can be significantly facilitated.

A 10% increase from the background optical density (O.D.), within a specified energy range, is established herein as criterion for determining the plasmon onset time t_0. Table I summarizes the averaged onset times, t_0, for each isothermal regime. The cited uncertainty in the last significant figure (the number in parenthesis) stems from the onset time measured in two samples.

Table I. SPR onset time and nucleation rate

Temperature, ^{o}C	530	540	550	560	570
t_0, min	359(7)	166(6)	106(4)	39(7)	36(5)
J, min^{-1}	0.00278(5)	0.006(1)	0.0094(4)	0.025(5)	0.027(4)

It is established herein that SPR starts to develop after a temperature-dependent induction time. This study proposes that during the induction period particles nucleate and grow. However, the growing particles do not become large enough for SPR to be detected. Hence, it is suggested that the nucleation process dominates the copper precipitation. Thus, the described induction period constitutes the first step in the precipitation process. In this study the induction period is coined *pre-plasmonic* period. The inverse of the SPR onset time can be associated to the Cu pre-plasmonic precipitation rate. In order to estimate the size of the smallest plasmonic copper particle, single-stage distribution analysis[17] is employed. Continuous nucleation and growth normally result in a broad distribution of particle sizes, i.e., the first nucleated particle has the largest size and so forth. If the particle growth rate is known, one can calculate the 'birth dates' of particles belonging to different size groups.[17] The particle growth rate is estimated herein assuming that the growth process is purely diffusion based one.[15] Therefore, the particle size is linear with the square root of time. The smallest Cu NP diameter giving rise to a detectable SPR was estimated to be the average particle diameter at the established SPR onset time t_0. The particle size distribution analysis herein employs the particle size HRTEM histogram, obtained after one hour of 600 °C HT process, Fig. 2. This study estimated that at the time of the onset of the SPR the average Cu NP size is ~1.5 nm. Since particles smaller than 1.5 nm cannot be detected spectroscopically, these particles might be considered as the optically critical ones. Hence, the classical nucleation theory can be applied for developing particles below this size.

It is known that the HRTEM imaged portion of the sample (right inset in Fig. 2), cannot be correlated directly with the spectroscopically probed area. The extinction spectra, shown in the left inset of the same figure, are taken from an area of ~10^4 μm^2. HRTEM imaging was performed afterward. The total sample area analyzed from the HRTEM images is less than 25 μm^2 (400 times smaller than the spectrally probed area). Therefore, Fig. 2 serves as a mere illustration of the isothermal precipitation end state. Mostly spherical particles with some size dispersion are observed. The average diameter is ~2.5 nm; and the average distance between the particles is estimated to be ~5.4 nm.

From the classical nucleation theory, the steady-state crystal nucleation rate, J (the number of critical clusters formed per unit time in a unit volume of the system) is proportional to a product of two terms profoundly affected by the temperature, T. The first term is thermodynamic in origin, controlled by the driving force of nucleation, ΔG^*. The second term is a kinetic term dependent on atomic diffusion. [27-30]

$$J(T) \propto \exp\left(\frac{-\Delta G^*}{k_B T}\right)\exp\left(\frac{-E_a}{k_B T}\right), \qquad (1)$$

where k_B is the Boltzmann constant; ΔG^* is the change of the Gibbs free energy, due to the formation of a critical cluster of the new phase. ΔG^* can be considered equal to the work for critical clusters formation, W_c and independent of the temperature in the studied temperature interval. In order to obtain information about the energy associated to the nucleation rate, Eq. (1) can be linearized:

$$\ln[J(T)] \propto -\left(\frac{W_c + E_a}{k_B}\right)\frac{1}{T}. \qquad (2)$$

The authors propose the linear form of Eq. (1), i.e. Eq. (2), to be used to a first approximation evaluation of the activation energy of the pre-plasmonic (optically critical) particle precipitation with temperature dependent rate $J(T)$. The pre-plasmonic precipitation rate is calculated as a reciprocal of the measured onset time, t_0.[17] The values of the rates for each isothermal process are listed in the third row in Table I. The apparent activation energy of the overall process would consist of two parts – work for critical cluster formation, W_c and diffusion kinetic barrier, E_a. A plot of ln [$J(T)$] *vs*. T^{-1} was obtained as shown in Fig. 3. From the slope of the linear fit, the overall apparent energy barrier, for optically critical (pre-plasmonic) particle in the phosphate

glass matrix is estimated to be 3.9(7) eV. The R^2 coefficient of determination, indication for the goodness of fit (solid lines in Fig. 3) is 0.958.

Further on, the peak optical density was recorded for each absorption spectrum, regardless of associated photon energy, within the specified range. Overall, the Cu NP SPR in the barium-phosphate matrix is located between 2.1 and 2.2 eV which happens to be slightly above the threshold energy for the interband transitions for Cu, 2.1 eV [31]. An SPR occurring above the interband transition onset leads to asymmetrical line shape and efficient plasmon dampening.[32] Spectroscopically the plasmon dampening is revealed by combination of plasmon peak height reduction and band broadening, Fig. 1. Under such circumstances relating the SPR FWHM to the reciprocal of the NP size[32] can be associated with a considerable uncertainty.

The second stage of the Cu NP precipitation is termed *plasmonic* precipitation. The peak optical density of the developed SPR (see inset of Fig. 4) follows a characteristic sigmoidal curve. The volume fraction (α_T) of the plasmonic copper precipitate is directly proportional to the measured peak O.D. In agreement with the KJMA phase transformation model the time evolution of $\alpha_T(t)$ during an isothermal process is:

$$\alpha_T(t - t_0) = 1 - e^{[-k_T(t-t_0)]^n}, \quad (3)$$

where k_T is the overall transformation rate at temperature T; t is the elapsed time; t_0 is the experimentally measured onset time (*vide supra*); n is an integer between 1 and 4, called the Avrami index. To a first approximation five peak O.D. isotherms at 530 ^{o}C, 540 ^{o}C, 550 ^{o}C, 560 ^{o}C and 570 ^{o}C are fitted using Eq. (3) linearized as:

$$\ln[-\ln[1 - \alpha_T(t - t_0)]] = n\ln(t - t_0) + nk_T. \quad (4)$$

Illustration of the three isothermal linear fits is presented in Fig. 4. The R^2 coefficient of determination, solid lines in Fig. 4 of each fit is 0.989, 0.987 and 0.985 for 530 °C, 550 °C and 570 °C, correspondingly. The filled symbols in the inset and those in the main figure are the same data points. The value of the slope is the Avrami index. Obtained indexes for each isotherm are summarized in the second row of Table II. The Avrami index varies between 2.7 and 3.8. No specific temperature trend is noticed with the temperature. Therefore, the average index of 2.8(6) has been evaluated as characteristic for the plasmonic stage applicable for the considered 40-degree interval. The reported data do not exclude the possibility of temperature

dependence of the Avrami index outside the measured temperature interval. Given the estimated uncertainty and considering that the KJMA model calls for an integer value: $n = 3$ can be suggested in agreement with the observed spherical (Fig. 2 right inset) particle growth.[17]

Table II. Avrami indexes and plasmonic phase precipitation rates, k_T

Temperature, ^{o}C	530	540	550	560	570
Avrami index, n	3.75(5)	2.7(1)	3.7(1)	2.9(1)	2.8(1)
k_T, min^{-1}	0.0044(5)	0.014(3)	0.013(2)	0.023(7)	0.032(1)

Further on, utilizing the linearized Avrami equation (Eq. 4) for each isothermal precipitation process with its corresponding index, the transformation rate, k_T, is evaluated for each temperature. Obtained plasmonic isothermal precipitation rates are summarized in the third row of Table II. It is noted that the plasmonic precipitation rate stays higher than the respective pre-plasmonic one, Table I. Hence, it can be suggested that spherical particle growth, rather than the nucleation dominates the copper precipitation during the second stage, as discussed in more detail below. In addition, both kinetic rates seem to increase approximately an order of magnitude from 530 ^{o}C to 570 ^{o}C which suggests that the basic atomic kinetic processes involved in the two stages are interrelated. The activation energy of the plasmonic E_a, can be evaluated utilizing the linear form of the Arrhenius equation:

$$\ln(k_T) = -\left(\frac{E_a}{R}\right)\frac{1}{T} + \ln A \,. \qquad (5)$$

Fig. 5 presents the linear Arrhenius plot. A value of 2.6(5) eV for the activation of the plasmonic precipitation of 10Cu/Sn in the barium-phosphate matrix has been estimated. The discussed isothermal experimental data of the studied precipitation do not rule out possible temperature dependence of the activation energy in a broader temperature range. It appears that the proposed method, applied in the relatively narrow 40-degree interval (530 – 570 ^{o}C), yields to a first approximation, within the experimental uncertainty, an activation energy independent of temperature.

According to nucleation and growth theory, the three stages associated with particle formation and growth processes are: 1) nucleation; 2) diffusion-based growth, which occurs at large supersaturation values; 3) Ostwald ripening (recondensation stage) which occurs, when the

concentration of the limiting reactant approaches the solubility limit. Due to continuous generation of limiting reactant Cu by reduction of ionic copper species with tin, large supersaturation values are expected in the glass system. Hence, no Ostwald ripening is expected in this glass system[33]. Therefore, nucleation and diffusion-based growth are the two microscopic mechanisms naturally leading to the decrease in supersaturation, and copper precipitation in its final form of spherical NPs. As the *in-situ* collected extinction spectra suggested, the isothermal precipitation can be discussed as two stage process: pre-plasmonic (atomic clusters, prior to the appearance of the SPR) and plasmonic phase (larger, plasmonic NPs). The spectroscopically separated stages agree with the established fact that the thermodynamic and kinetic parameters may change significantly in dependence on cluster and nanoparticle size[17]. Consequently, the estimates of these parameters obtained from nucleation data (pre-plasmonic stage) may not be appropriate for the description of growth processes of NPs (plasmonic stage). As discussed above, the pre-plasmonic stage activation energy was dominated by critical nuclei formation, while the plasmonic stage seems to be controlled predominantly via plasmonic particle growth. It can be suggested that a rough estimate of the critical nuclei formation work W_c contribution in the pre-plasmonic stage can be estimated by the difference between the apparent overall pre-plasmonic and plasmonic activation energies, to be 1.3(9) eV.

Most importantly, the value of the plasmonic precipitation activation energy estimated in 10Cu/Sn doped barium-phosphate glass (2.6 eV) is in a good agreement with the previously estimated values of the diffusion activation energy during isothermal NP growth of 8 mol.% Ag/Sn and 4 mol. % Ag/Sn in aluminophosphate matrix, 3.2 eV [34] and 5.2 eV, [15] respectively. Furthermore, the measured herein glass transition temperature T_g of each nanocomposite is related to the diffusion activation energy in the same material. A manifested tendency of the diffusion activation energy to decrease with the Ag and Sn doping concentration in relation to the glass transition temperature reduction in the aluminophosphate matrix is plotted in Fig. 6 (square symbols). Similar tendency of T_g of the xSnO-60ZnO-40P_2O_5 (SZP) glasses as a function of SnO content is reported by Masai et al.[35] The plasmonic precipitation activation energy for the Cu precipitation in 10Cu/Sn barium-phosphate glass is plotted on the same graph with a solid circle symbol. Intriguingly, the new value lies on the same line with correlation

factor of 0.9998. As a consequence, an empirical linear proportionality between the diffusion activation energy, E_a (eV) and T_g (K) is proposed as:

$$E_a = A * k_B (T_g - T_c), \quad (6)$$

where A is unitless empirical parameter and k_B is the Boltzman constant in eV/K. In case of metal atoms (Cu, Ag) in phosphate glass network, A is estimated to be 505(10). T_c is another experimentally determined temperature parameter, evaluated to be 664(1) K. Eq. (5) could be justified based on the direct increase of the E_a and T_g, with the average bond strength. A Raman spectroscopy study testing the hypothesis of structural alteration due to increased average bond strength has been carried out. The inset in Fig 6 compares the Raman spectra of the 4Ag/Sn in aluminophosphate matrix and the 10Cu/Sn in barium-phosphate matrix. The shift to higher wavenumbers of the symmetric stretching modes of the bridging, ν_s(POP) and non-bridging oxygen $\nu_s(PO_2)$ presents a direct evidence for a stronger covalent bond in the phosphate network.[36-38] The stronger covalent bond undoubtedly affects the network structure rigidity and, by extension T_g. Further theoretical and experimental work is underway for expanding the range of applicability of Eq. (6). The importance of the proposed empirical dependence, Eq. (6), stems from the fact that it relates a routinely measured macroscopic parameter, T_g, to an atomic kinetic parameter, E_a, of which evaluation is not trivial.

Conclusions

Quantitative copper nanoparticle precipitation kinetics in a melt-quenched barium-phosphate glass matrix has been studied by *in situ* isothermal optical microspectroscopy. Proposed is a viable experimental method for overcoming the inherent technological and spectroscopic challenges in the study of Cu NPs. Two precipitation stages are suggested to facilitate the employment of the classical nucleation and growth theory, and the phase change Kolmogorov−Johnson−Mehl−Avrami model. Activation energy of 3.9(7) eV and 2.6(5) eV has been estimated for the pre-plasmonic and plasmonic precipitation regimes, respectively. The difference of the two values can be used as a good estimate of the Gibbs free energy for critical nuclei formation as 1.3(9) eV.

The study was validated by independent techniques supporting the obtained value of the activation energy of the Cu particle precipitation in connection to glass structural and thermal properties. The empirically-derived Eq. (6) is a novel contribution to solid-state kinetics of nanocomposite materials. The proposed direct relationship suggests the feasibility for estimating the diffusion activation energy from a routinely measured macroscopic parameter, the glass transition temperature.

Acknowledgements

M. Sendova thanks the undergraduate students Abigail McAloon, for collecting some of the optical density spectra and Ralf Raud, for obtaining the T_g values. Research was partially sponsored by the Army Research Laboratory under Cooperative Agreement Number W911NF-09-2-0004 and a private grant from George and Tina Skestos.

References

1 M. L. Brongersma and V. M. Shalaev, *Science,* 2010, **328**, 440 - 441.

2 J. N. Anker, W. P. Hall, O. Lyandre, N. C. Shah, J. Zhao and R. P. Duyne, *Nat. Mater,.* 2008, **7**, 442.

3 H. A. Atwater and A. Polman, *Nat. Mater*., 2010, **9**, 205.

4 L. Esteban-Tejeda, F. Malpartida, A. Esteban-Cubillo, C. Pecharromán and J.S. Moya, *Nanotechnology,* 2009, **20**, 505701.

5 O. Rubilar, M. Rai, G. Tortella, M.C. Diez, A.B. Seabra and N. Duran, *Biotechnol. Lett.,* 2013, **35**, 1365.

6 J. A. Jimenez, S. Lysenko, G. Zhang and H. Liu, *J. Mater. Sci.,* 2007, **43**, 1856.

7 A. Miotello, G. D. Marchi, G. Mattei, P. Mazzoldi and A. Quaranta, *Appl. Phys. A*., 2000, **70**, 415.

8 G. Kellermann and A.F. Craievich, *Crystallography Reports,* 2008, **53**, 1241.

9 P. Gangaopadhayay, P. Magudapathy, R. Kesavamoorthy, B.K. Panigrahi, K.G. M. Nair and P.V. Satyam, *Chem. Phys. Lett*., 2004, **388**, 416.

10 M. Sendova and J. A. Jiménez, *J. Phys. Chem*. C., 2012, **116**, 17764.

11 D. A. Rayan, Y. H. Elbashar, M. M. Rahad and A. El-Korashy, *J. Non-Cryst. Solids,* 2013, **382**, 52.

12 K. E. Lipinkska-Kalita, D. M. Krol, R. J. Hemley, G. Mariotto, P. E. Kalita and Y. Ohki, *J. Appl. Phys.,* 2005, **98**.

13 R. Kibar, A. Çetin and N. Can, *Physica B,* 2008, **404**, 105.

14 R. Udayabhaskar, B. Karthikeyan and M. S. Ollakkan, *Plasmonics,* 2014, **9**, 553.

15 J. A. Jiménez and M. Sendova, *Chem. Phys. Lett*., 2011, **503**, 283.

16 J. A. Jiménez, M. Sendova and M. Sendova-Vassileva, *ACS – Appl. Mater. Interfaces,* 2011, **3**, 447.

17 V. M. Fokin, E.D. Zanotto, N. S. Yuritsyn and J. W. P. Schmelzer, *J. Non-Cryst. Solids*., 2006, **352**, 2681.

18 A. N. Kolmogorov, *Izv. Akad. Nauk SSSR, Ser. Matem*. 1937, **3**, 355.

19 M. Avrami, *J. Chem. Phys.,* 1939, **7**, 1103.

20 W. A. Johnson and R. F. Mehl, *Trans. AIME,* 1939, **135**, 416.

21 J. A. Jiménez, *J. Mater. Sci*. 2014, **49**, 4387.

22 A. G. S. Masaaki Sugiyama, *J. Electron Micros.,* 2004, **53**, 527.

23 N. Kato, *J. Electron Microsc.,* 2004, **53**, 451.

24 B. Ghosh, P. Chakraborty, B. P. Singh and T. Kundu, *Appl. Surf. Sci.,* 2009, **256**, 289.

25 Y. Xia, Y. Xiong, B. Lim and S. E. Skrabalak, *Angew. Chem. Int. Ed.* 2008, **48**, 60.

26 G. Walters and I. P. Parkin, *J. Mater. Chem*., 2009, **19**, 574.

27 J. W. P. Schmelzer, *J. Non-Cryst. Solids* 2008, **354**, 269.

28 A. Putnis, *An Introduction to Mineral Sciences*; Cambridge University Press: Cambridge, 1992.

29 M. Volmer and A. Weber, *Z. Phys. Chem,.* 1925, **119**, 277.

30 L. Farkas, *Z. Physikal. Chemie,* 1927, **125**, 236.

31 H. Ehrenreich and H. R. Phillip, *Phys. Rev.,* 1962, **128**, 1622.

32 U. Kreibig and M. Vollmer, *Optical Properties of Metal Clusters*; Springer: Berlin, 1995.

33 J. A. Jiménez, M. Sendova, H. Liu and F. E. Fernández, *Plasmonics* 2011, **6**, 399.

34 J. A. Jiménez, M. Sendova and H. Liu, *J. Lumin.* 2011, **131**, 535.

35 H. Masai, Y. Takahashi, T. Fujiwara, S. Matsumoto, Y. Tokuda and T. Yoko, *Optics Express,* 2012, **3**, 27319.

36 L. B. Fletcher, J. J. Witcher, W. B Reichman, A. Arai, J. Bovatsek and D. M. Krol, *J. Appl. Phys.,* 2009, **106**, 083107.

37 D. Ilieva, B. Jivov, C.P. Bogachev, I. Penkov and Y. Dimitriev, *J. Non-Cryst. Solids,* 2001, **283**, 195.

38 R. Brow, *J. Non-Cryst., Solids,* 2000, **1**,263-264.

Figure captions

Figure 1. Real-time SPR band evolution of Cu nanocomposite glass monitored during HT at 4 min intervals from 52 to 96 minutes at 560 °C. The interband transitions for Cu, 2.1 eV are indicated by the vertical dashed line.

Figure 2. Particle size distribution histogram; TEM image (right inset); O.D. spectra from the same sample prior to the TEM

Figure 3. Arrhenius plot of the pre-plasmonic precipitation rates (Table I)

Figure 4. Peak O.D. as a function of time for the indicated isothermal settings (inset). Linearized Avrami plots for a subset (solid symbols) of the same data.

Figure 5. Arrhenius plot of the plasmonic precipitation rates (Table II).

Figure 6. Linear relationship between diffusion activation energy and T_g. In the inset, the Raman spectra of the 4Ag/Sn aluminophosphate glass (black solid trace) and 10Cu/Sn in barium-phosphate glass (red solid trace) are compared.

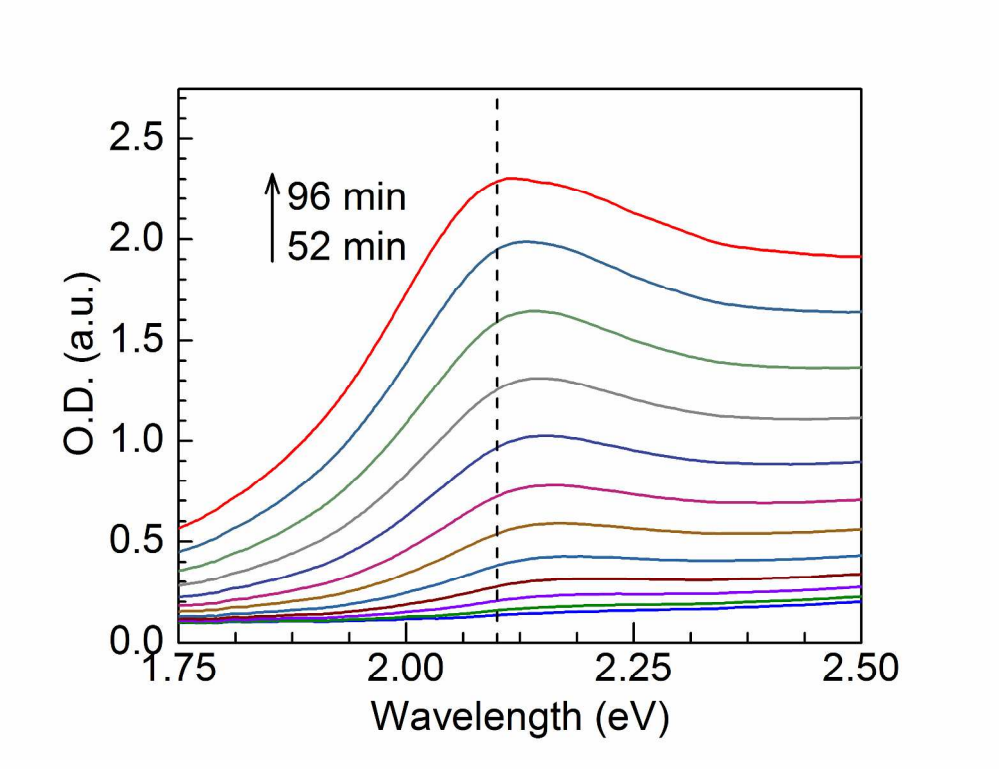

Figure 1. Real-time SPR band evolution of Cu nanocomposite glass monitored during HT at 4 min intervals from 52 to 96 minutes at 560 °C. The interband transitions for Cu, 2.1 eV are indicated by the vertical dashed line.
279x215mm (300 x 300 DPI)

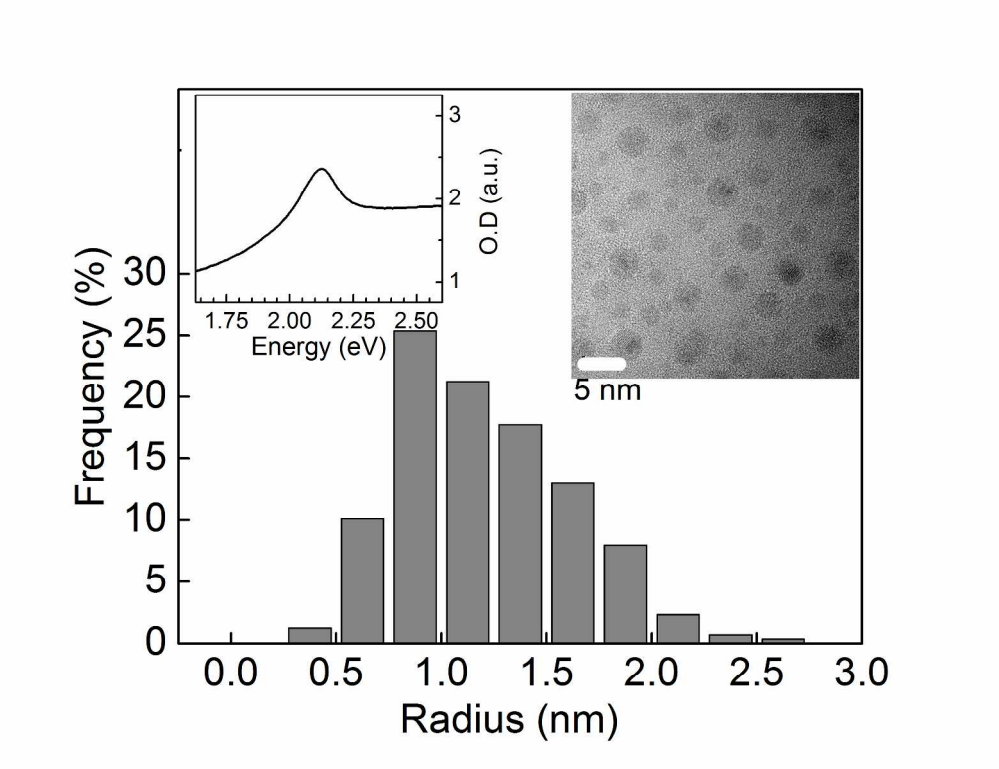

Figure 2. Particle size distribution histogram; TEM image (right inset); O.D. spectra from the same sample prior to the TEM
279x215mm (300 x 300 DPI)

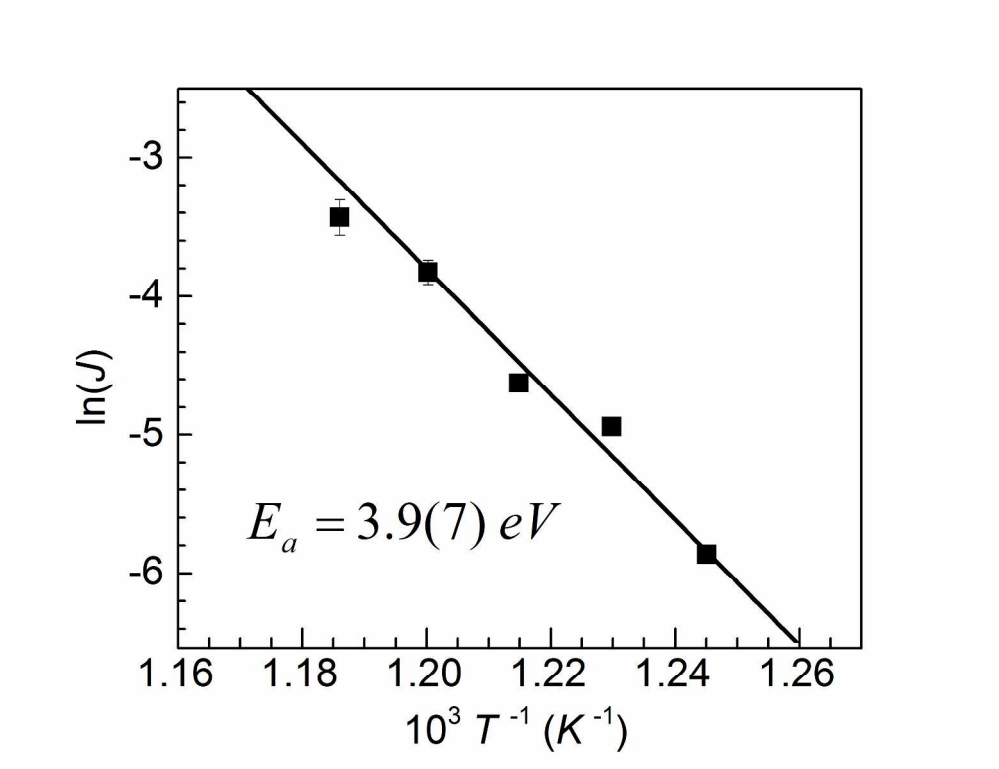

Figure 3. Arrhenius plot of the pre-plasmonic precipitation rates (Table I)
279x215mm (300 x 300 DPI)

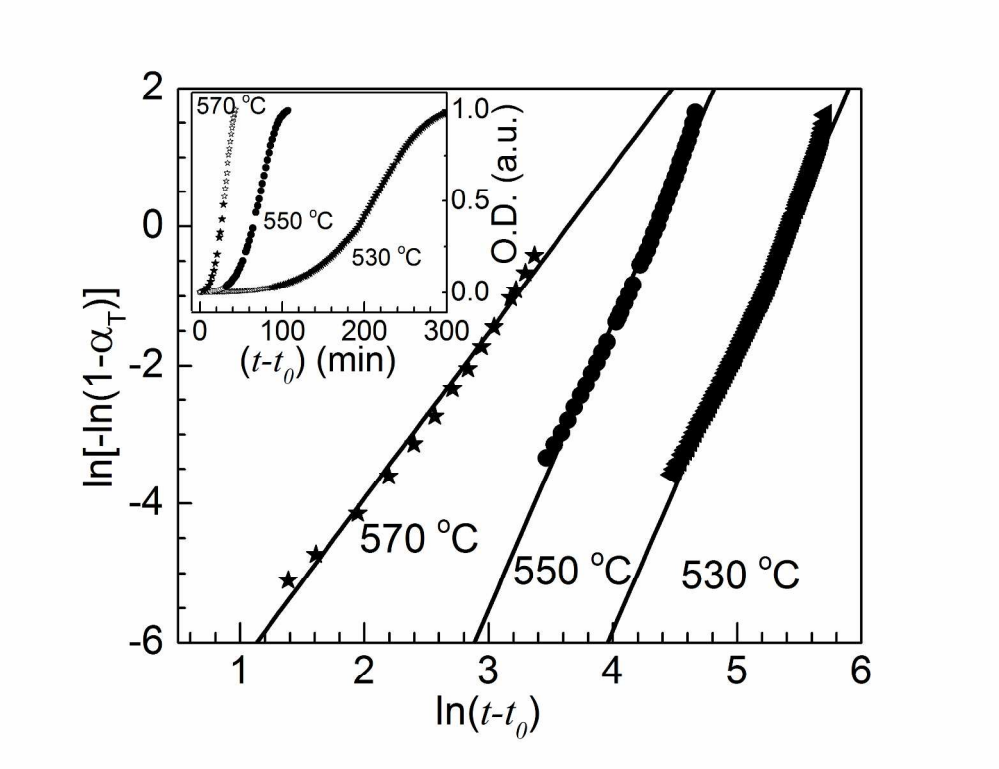

Figure 4. Peak O.D. as a function of time for the indicated isothermal settings (inset). Linearized Avrami plots for a subset (solid symbols) of the same data.
279x215mm (300 x 300 DPI)

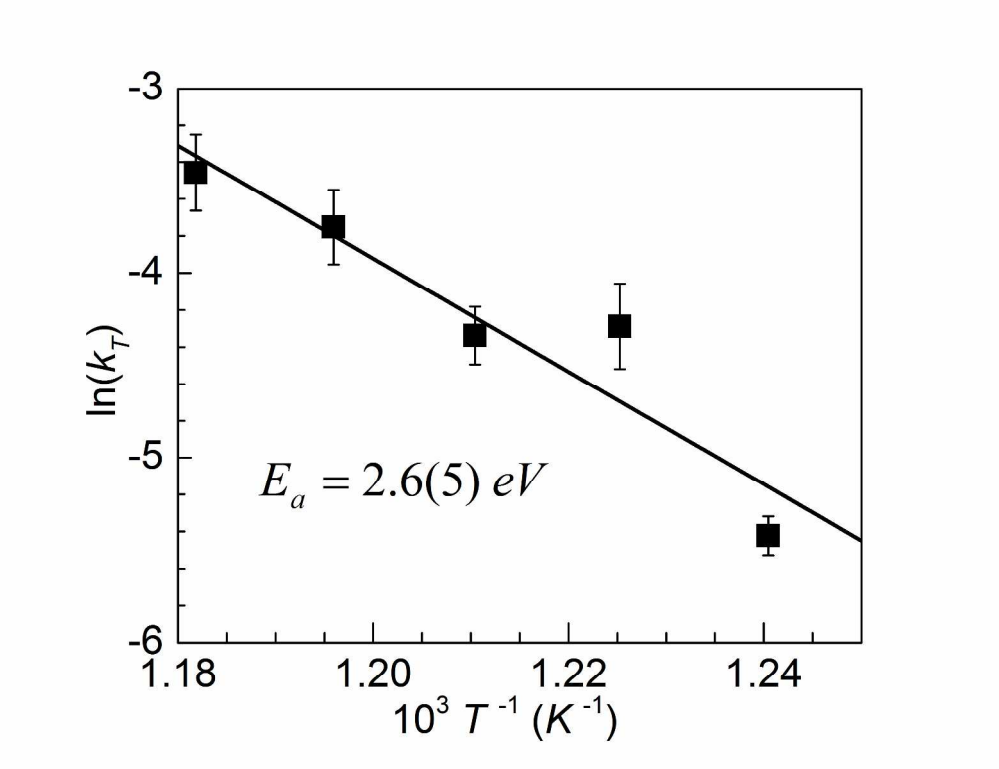

Figure 5. Arrhenius plot of the plasmonic precipitation rates (Table II).
279x215mm (300 x 300 DPI)

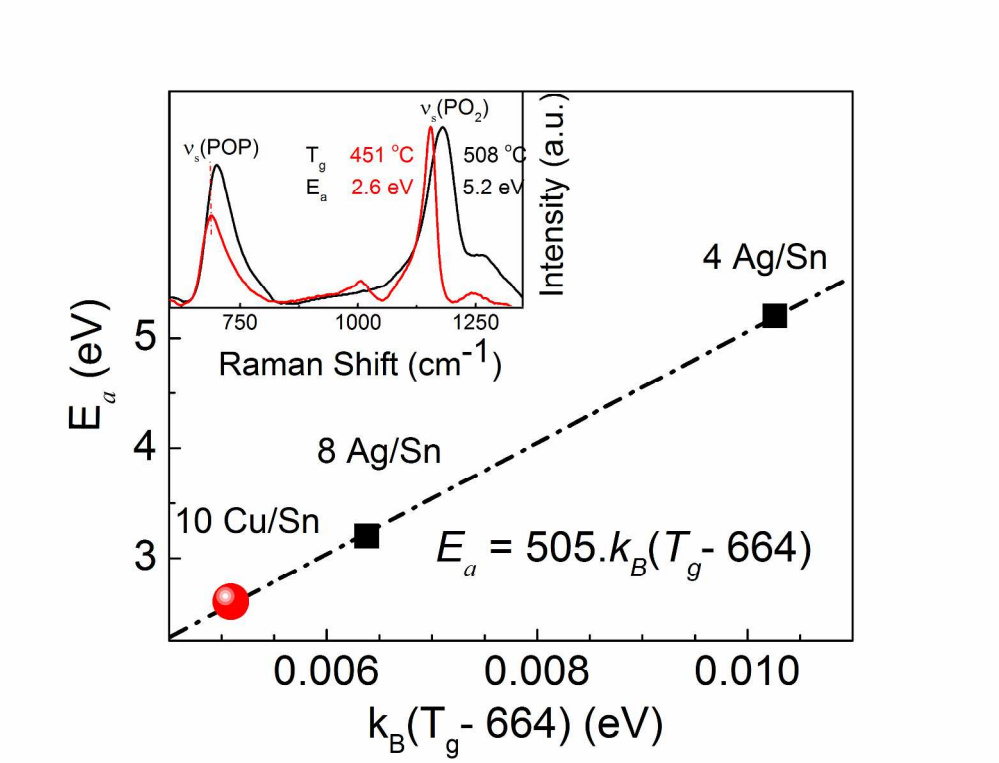

Figure 6. Linear relationship between diffusion activation energy and Tg. In the inset, the Raman spectra of the 4Ag/Sn aluminophosphate glass (black solid trace) and 10Cu/Sn in barium-phosphate glass (red solid trace) are compared.
264x203mm (300 x 300 DPI)